MOX-Report No. 03/2020

Compliance-stress constrained mass minimization for topology optimization on anisotropic meshes

Ferro, N.; Micheletti, S.; Perotto, S.

MOX, Dipartimento di Matematica
Politecnico di Milano, Via Bonardi 9 - 20133 Milano (Italy)

mox-dmat@polimi.it http://mox.polimi.it

Compliance-stress constrained mass minimization for topology optimization on anisotropic meshes

Nicola Ferro[#], Stefano Micheletti[#], Simona Perotto[#]

January 6, 2020

[#] MOX– Modellistica e Calcolo Scientifico
Dipartimento di Matematica, Politecnico di Milano
Piazza L. da Vinci 32, I-20133 Milano, Italy
{nicola.ferro,stefano.micheletti,simona.perotto}@polimi.it

Abstract

In this paper, we generalize the SIMPATY algorithm, which combines the SIMP method with anisotropic mesh adaptation to solve the minimum compliance problem with a mass costraint. In particular, the mass of the final layout is now minimized and both a maximum compliance and a maximum stress can be enforced as either mono- or multi-constraints. The new algorithm, named MSC-SIMPATY, is able to sharply detect the material-void interface, thanks to the anisotropic mesh adaptation. The presented test cases deal with three different scenarios, with a focus on the effect of the constraints on the final layouts and on the performance of the algorithm.

Keywords: Topology optimization – Stress constraint – Anisotropic mesh adaptation

1 Introduction

Topology optimization is of utmost interest in different branches of industrial design, such as biomedical, space, automotive, mechanical, architecture (see, e.g., [27, 37, 11, 54, 20]). Similar formulations can also be adopted for the optimization of structures in different contexts, from fluid-structure interaction to the tailored design of magnetic or auxetic metamaterials [53, 33, 46, 23].

One aims at minimizing (or maximizing) a quantity of interest under specific design constraints, which may be interchanged according to the considered field of application. A standard context leads to minimize the compliance of a structure for a given mass (to optimize the structure performance at a given cost) or, vice versa, to minimize the weight under a

prescribed compliance (to produce a lightweight structure characterized by a desired stiffness).

Independently of the number of possible design specifications, we are led to solve a constrained optimization problem, possibly in an efficient way with a view to the manufacturing process. Several methods are available in the literature driving topology optimization. Among these, we mention the density-based approaches [6, 8, 45], the level-set methods [4, 38], topological derivative procedures [48], phase field techniques [17, 10], evolutionary approaches [52], homogenization [7, 3], performance-based optimization [36]. We focus on the first class and, in particular, on the SIMP (Solid Isotropic Material with Penalization) method [7, 8, 45] where the material distribution is modeled via an auxiliary scalar field, referred to as density, taking values between zero (void) and one (material) in the design domain.

In some recent papers, a new algorithm, called SIMPATY (SIMP with AdaptiviTY), has been proposed to offer an efficient design tool for 3D printing [43, 42]. SIMPATY algorithm combines SIMP method with an advanced mesh adaptation technique based on an a posteriori recovery-based error analysis [55, 56]. In particular, the authors employ anisotropic triangular meshes [25, 24]. This choice leads to a very cost-effective procedure, which alleviates the end user from most of the post-processing step, towards the free-form design [43, 22, 23]. The setting considered in these papers addresses the minimization of the compliance under a mass constraint.

In this paper, we move to a more general framework with a view to more complex applications, by minimizing the structure mass given a maximum stress and/or a maximum compliance as a mono- or multi-constraint. The control on the stress takes into account a real requirement in many contexts, since it allows us not to overcome a maximum limit for the mechanical resistance of the material [12, 34]. The SIMPATY algorithm is here modified into the MSC-SIMPATY (Mass-Stress-Compliance SIMPATY) procedure to tackle the new optimization setting. The numerical verification, despite preliminary, meets the expectation. The designed layouts do depend on the considered constraints, and only a bound on both compliance and stress delivers a structure that is sufficiently stiff as well as failure-free under the applied loads. Moreover, the stress constraint turns out to be more hard to deal with, since the nonlinearities involved in the corresponding definition make the convergence of SIMPATY slower. In all cases, however, the predicted layouts are characterized by sharp interfaces between void and material, with no jagged boundaries, thanks to the employment of anisotropic meshes, which are tailored to the density profile. This also makes the final layouts almost ready for 3D printing, as shown by the .STL files in Figure 8.

The layout of the paper is the following. Section 2 details the SIMP-based topology optimization procedure, whereas Section 3 deals with the corresponding numerical discretization. Section 4 focuses on the MSC-SIMPATY algorithm, first by introducing the optimization algorithm and

then the mesh adaptation procedure. Section 5 gathers some numerical tests, which alternate mono- with multi-constrained problems. Finally, some conclusions are drawn in the last section.

2 The mathematical model

Several methods are available in the literature to identify the topologically optimal structure, contained in the initial domain and subject to design constraints. Among these, we cite approaches based on phase-field [15, 10, 17], level set [2, 13, 14], density-based methods [6, 8, 45], and more recent techniques [50, 28, 44, 29]. In this paper, we adopt the SIMP (Solid Isotropic Material with Penalization) formulation [8].

2.1 The SIMP linear elasticity equation

In a structure optimization setting, the standard mathematical model is represented by the linear elasticity problem [30], i.e.,

$$\begin{cases} -\nabla \cdot \sigma(\mathbf{u}) = \mathbf{0} & \text{in } \Omega \\ \mathbf{u} = \mathbf{0} & \text{on } \Gamma_D \\ \sigma(\mathbf{u})\mathbf{n} = \mathbf{f} & \text{on } \Gamma_N \\ \sigma(\mathbf{u})\mathbf{n} = \mathbf{0} & \text{on } \Gamma_F, \end{cases} \tag{1}$$

where $\Omega \subset \mathbb{R}^2$, $\mathbf{u}$ is the displacement, $\sigma(\mathbf{u}) = 2\mu\varepsilon(\mathbf{u}) + \lambda I : \varepsilon(\mathbf{u})$ is the stress tensor for an isotropic material, with $\varepsilon(\mathbf{u}) = \big(\nabla\mathbf{u} + (\nabla\mathbf{u})^T\big)/2$ the small displacement strain tensor,

$$\lambda = \frac{E\nu}{(1+\nu)(1-2\nu)}, \quad \mu = \frac{E}{2(1+\nu)}$$

the Lamé coefficients, with E the Young modulus, ν the Poisson ratio and I the identity tensor, $\mathbf{f} : \Gamma_N \to \mathbb{R}^2$, is the load applied to a portion Γ_N of the boundary, $\mathbf{n}$ is the unit outward normal vector to $\partial\Omega$, Γ_D is the portion of the boundary where the structure is clamped, and Γ_F is the normal stress-free boundary, such that $\Gamma_D \cup \Gamma_N \cup \Gamma_F = \partial\Omega$.

The weak form of problem (1) is: find $\mathbf{u} \in U = \{\mathbf{v} \in [H^1(\Omega)]^2 : \mathbf{v} = \mathbf{0} \text{ on } \Gamma_D\}$, s.t.

$$a(\mathbf{u}, \mathbf{v}) = \mathcal{G}(\mathbf{v}) \quad \forall \mathbf{v} \in U, \tag{2}$$

with

$$a(\mathbf{u}, \mathbf{v}) = \int_\Omega \sigma(\mathbf{u}) : \varepsilon(\mathbf{v})\, d\Omega, \quad \mathcal{G}(\mathbf{v}) = \int_{\Gamma_N} \mathbf{f} \cdot \mathbf{v}\, d\gamma.$$

The SIMP method modifies the elasticity equation by weighting (2) via the density function ρ, i.e., a continuous design variable, modeling the distribution of material in the design domain. A priori, the density is assumed

to be a function in $L^\infty(\Omega)$, taking values in the interval $[0,1]$, with the understanding that $\rho = 0$ represents the void and $\rho = 1$ the full material. To avoid nonphysical intermediate densities, the SIMP formulation actually resorts to a suitable power-law penalization on ρ, namely ρ^p with $p \geq \max\{2/(1-\nu), 4/(1+\nu)\}$, which promotes the extreme values, 0 and 1 [8, 5].

The SIMP linear elasticity equation is thus: find $\mathbf{u} \in U$ s.t.

$$a_\rho(\mathbf{u}, \mathbf{v}) = \mathcal{G}(\mathbf{v}) \quad \forall \mathbf{v} \in U, \tag{3}$$

with

$$a_\rho(\mathbf{u}, \mathbf{v}) = \int_\Omega \sigma_\rho(\mathbf{u}) : \varepsilon(\mathbf{v})\, d\Omega, \tag{4}$$

and $\sigma_\rho(\mathbf{u}) = \rho^p \big[2\mu\varepsilon(\mathbf{u}) + \lambda I : \varepsilon(\mathbf{u})\big]$. Notice that the penalization modifies the material properties weighting the Lamé coefficients.

2.2 The topology optimization

To formalize the topology optimization, we have to introduce a cost functional, $\mathcal{J}$, to be minimized, as well as prescribed constraints. A standard choice for $\mathcal{J}$ is the static compliance of the structure, or the total mass of the final layout. Concerning the constraints, (3) can be used to take into account the physical model at hand, whereas other constraints are added to include design specifications, such as an upper bound on the local stresses or on the fundamental frequency of vibration. According to the application of interest, cost functional and constraints can become interchangeable.

Thus, a general topology optimization problem can be formulated as: find $\rho \in L^\infty(\Omega)$ s.t.

$$\min_{\rho \in L^\infty(\Omega)} \mathcal{J}(\mathbf{u}(\rho), \rho) \ : \begin{cases} a_\rho(\mathbf{u}(\rho), \mathbf{v}) = \mathcal{G}(\mathbf{v}) \ \forall \mathbf{v} \in U \\ C_i(\mathbf{u}(\rho), \rho) \leq c_i, \ i = 1, \ldots, n_C \\ \rho_{\min} \leq \rho \leq 1, \end{cases} \tag{5}$$

where $C_i(\mathbf{u}(\rho), \rho) \leq c_i$ enforces a generic inequality constraint, with c_i the corresponding upper bound and n_C the total number of constraints, while the two-sided inequality ensures the elasticity system in (3) to be well-defined, with $0 < \rho_{\min} < 1$.

In previous works, we focused on the minimization of the compliance, $\mathcal{C}$, subject to a maximum allowable mass [23, 22, 43], so that $\mathcal{J} = \mathcal{C}$, $n_C = 1$, $C_1 = \mathcal{M}$, with

$$\mathcal{C}(\mathbf{u}(\rho), \rho) = \mathcal{C}(\mathbf{u}(\rho)) = \int_{\Gamma_N} \mathbf{f} \cdot \mathbf{u}(\rho)\ d\gamma, \tag{6}$$

$$\mathcal{M}(\mathbf{u}(\rho), \rho) = \mathcal{M}(\rho) = \frac{1}{|\Omega|} \int_\Omega \rho\, d\Omega, \tag{7}$$

the volume fraction set to a desired value c_1.

The goal pursued in this paper is more challenging, since we are interested in solving a multi-constrained optimization problem. In particular, we set in (5) $\mathcal{J} = \mathcal{M}$, $n_C = 2$, $C_1 = \mathcal{S}$ and $C_2 = \mathcal{C}$, where

$$\mathcal{S}(\mathbf{u}(\rho), \rho) = ||\sigma_{VM}(\mathbf{u}(\rho), \rho)||_{L^\gamma(\Omega)} \tag{8}$$

approximates the maximum density-weighted von Mises stress

$$\sigma_{VM}(\mathbf{u}(\rho), \rho) = \rho^{p_s} E \sqrt{\varepsilon_{11}^2 + \varepsilon_{22}^2 - \varepsilon_{11}\varepsilon_{22} + 3\varepsilon_{12}^2},$$

being γ as large as possible [34], with ε_{ij} the ij-th component of the strain tensor, and p_s an exponent penalizing intermediate densities, but possibly different from p used in (4). Actually, several approaches are available in the literature to formalize the dependence of the stress field on the design variable, essentially adopting different penalizations [16, 15, 12]. The choice in (8) is the most straightforward one in view of the employment of the SIMP method. Thus, problem (5) becomes: find $\rho \in L^\infty(\Omega)$ s.t.

$$\min_{\rho \in L^\infty(\Omega)} \mathcal{M}(\rho) \ : \begin{cases} a_\rho(\mathbf{u}(\rho), \mathbf{v}) = \mathcal{G}(\mathbf{v}) \ \forall \mathbf{v} \in U \\ \mathcal{S}(\mathbf{u}(\rho), \rho) \leq S_{\max} \\ \mathcal{C}(\mathbf{u}(\rho)) \leq C_{\max} \\ \rho_{\min} \leq \rho \leq 1, \end{cases} \tag{9}$$

with $C_{\max}$ and $S_{\max}$ a maximum upper bound on the compliance and stress, respectively. Problem (9) amounts to minimizing the mass of the structure while ensuring a certain stiffness and stress.

3 The numerical discretization

We resort to a standard finite element approximation in order to numerically solve problem (9). This yields the discrete formulation: find $\rho_h \in V_h^r$ s.t.

$$\min_{\rho_h \in V_h^r} \mathcal{M}(\rho_h) \ : \begin{cases} a_\rho(\mathbf{u}_h(\rho_h), \mathbf{v}_h) = \mathcal{G}(\mathbf{v}_h) \ \forall \mathbf{v}_h \in U_h^s \\ \mathcal{S}(\mathbf{u}_h(\rho_h), \rho_h) \leq S_{\max} \\ \mathcal{C}(\mathbf{u}_h(\rho_h)) \leq C_{\max} \\ \rho_{\min} \leq \rho_h \leq 1, \end{cases} \tag{10}$$

where it is understood that $\mathbf{u}_h(\rho_h) \in U_h^s$, and U_h^s and V_h^r are the finite element spaces of vector and scalar functions of degree s and r, respectively, associated with a conforming triangular tessellation, $\mathcal{T}_h$, of the domain Ω [19].

Formulation (10) usually exhibits some drawbacks, the two main being the dependency of the optimal layout on the computational mesh and the presence of checkerboards, namely, of alternating solid and void elements in

a checkerboard pattern [8, 47]. The first issue is a consequence of the non-uniqueness of the solution to the optimization problem, while the second one depends on the two-field (density-displacement) formulation. Explicit limitations and filtering of the density distribution mitigate these two concerns [35, 9]. Another possible solution to checkerboards consists in using higher order finite elements for the displacement with respect to the density (i.e., we set $s \geq r$ in (10)). On the contrary, the non-uniqueness of the solution remains an issue, whatever the selected discretization.

Other minor issues of formulation (10) are grayscale (presence of intermediate densities) and staircase (jagged boundaries at the void-material interfaces) effects, and the geometric complexity of the final design (thin struts hard to be 3D-printed).
In [43], a new method is proposed to tackle the two last issues. The authors prove the effectiveness of SIMPATY algorithm, which merges the SIMP approach with an anisotropic mesh adaptation. SIMPATY provides a mesh fitting the sharp gradients of the density, possibly without any filtering. This allows us to drastically reduce any post-processing before manufacturing [42], in contrast to standard topology optimization softwares. Moreover, mesh adaptation admits the employment of linear finite elements for the $(\mathbf{u}(\rho), \rho)$ pair, without giving rise to undesirable checkerboards. Finally, this new design paradigm enables us to move towards a free-form design, both at a macro- and at a micro-scale [43, 23, 22].

4 The MSC-SIMPATY algorithm

The MSC (Mass-Stress-Compliance) variant of the SIMPATY algorithm alternates a minimization and a mesh adaptation step, separately detailed in the next two sections.

4.1 The optimization procedure

Two recurrent numerical methods to tackle problem (10) are the Interior Point OPTimizer (IPOPT) [51] and the MMA [49] algorithms. We choose IPOPT, being directly embedded in the software `FreeFem++`[32], which is a very handy tool both to discretize variational formulations and to efficiently manage metric-based mesh adaptation procedures.

IPOPT is a large-scale nonlinear optimization package, which includes both equality and inequality constraints via suitable slack variables. With reference to the generic problem (5), the main parameters to be passed to IPOPT are the functional $\mathcal{J}$, the quantities, C_i, c_i, $\rho_{\min}$, involved in the constraints, the gradient of the functional and of the constraints with respect to ρ, the initial guess, ρ_h^0, together with the maximum number, `Mit`, of iterations and the tolerance, `TOPT`, for the built-in stopping criterion. Actually, at this stage, all the involved functionals have to be meant as

functions of ρ, and the SIMP linear elastic equation in $(5)_1$ is taken into account explicitly, so that $\rho \mapsto \mathbf{u}(\rho)$ identifies the solution map. Moreover, the gradients are computed via a standard Lagrangian approach [43, 8]. Thus, the basic command syntax for IPOPT is

$$\texttt{IPOPT}(\mathcal{J}, \nabla_\rho \mathcal{J}, C_i, \nabla_\rho C_i, \rho_h^0, \rho_{\min}, c_i, \texttt{Mit}, \texttt{TOPT}, ...).$$

Other parameters can be added to this basic call (we refer to [51] for further details). The output of `IPOPT` is the optimal density.

4.2 The anisotropic mesh adaptation procedure

The adapted anisotropic mesh is generated by a metric-based procedure [26], driven by an a posteriori error estimator [1]. In particular, we resort to an anisotropic variant of the Zienkiewicz-Zhu estimator, η, to efficiently estimate the H^1-seminorm of the discretization error, $||\nabla\rho - \nabla\rho_h||_{L^2(\Omega)}$, associated with the density [55]. The rationale behind this choice is that we do expect large values for the H^1-seminorm of such an error where the density exhibits steep gradients, i.e., across the material-void interfaces. It is well known that anisotropic meshes are an ideal tool to detect sharp directional features [31, 18]. Moreover, recovery-based error estimators are very cheap to implement and quite general, depending only on the density and not on the target criteria.

Following [40], the error estimator coincides with $\eta^2 = \sum_{K\in\mathcal{T}_h} \eta_K^2$, with

$$\eta_K^2 = \frac{1}{\lambda_{1,K}\lambda_{2,K}} \sum_{i=1}^{2} \lambda_{i,K}^2 \left(\mathbf{r}_{i,K}^T\, G_{\Delta_K}\big(E_\nabla\big)\mathbf{r}_{i,K}\right), \tag{11}$$

where $\lambda_{i,K}$ and $\mathbf{r}_{i,K}$ represent the anisotropic information required to build the adapted mesh. In particular, $\lambda_{i,K}$, with $\lambda_{1,K} \geq \lambda_{2,K}$, measure the lengths of the semi-axes of the ellipse circumscribed to the generic element K of $\mathcal{T}_h$, while $\mathbf{r}_{i,K}$ provide the direction of the corresponding axes. The lengths $\lambda_{i,K}$ can be employed to measure the deformation of K, i.e., the aspect ratio $s_K = \lambda_{1,K}/\lambda_{2,K} \geq 1$. Moreover, $E_\nabla = \big[P(\nabla\rho_h) - \nabla\rho_h\big]_{\Delta_K}$ denotes the recovered error, i.e., the mismatch between the exact discrete gradient, $\nabla\rho_h$, and the recovered gradient,

$$P(\nabla\rho_h)|_{\Delta_K} = |\Delta_K|^{-1} \sum_{T\in\Delta_K} |T|\nabla\rho_h|_T,$$

coinciding with the area-weighted average of the discrete gradient on the patch Δ_K of the elements sharing at least a vertex with K [40, 21, 41]. Finally, $G_{\Delta_K}(\cdot) \in \mathbb{R}^{2\times 2}$ is a symmetric positive semidefinite matrix with entries

$$[G_{\Delta_K}(\mathbf{w})]_{i,j} = \sum_{T\in\Delta_K} \int_T w_i\, w_j\, dT \quad \text{with } i,j = 1,2, \tag{12}$$

for any vector-valued function $\mathbf{w} = (w_1, w_2)^T \in [L^2(\Omega)]^2$.

The local estimator, η_K, is now used in a predictive way to compute an optimal metric, minimizing the cardinality, $\#\mathcal{T}_h$, of the new mesh, and satisfying an error equidistribution criterion,

$$\eta_k^2 \simeq \frac{\texttt{TAD}^2}{\#\mathcal{T}_h}, \tag{13}$$

with TAD the desired accuracy on the global estimator η. These two requirements lead to solve an elementwise constrained optimization problem, which admits a unique explicit solution [40, 41],

$$\begin{cases} \lambda_{1,K}^{opt} = g_2^{-1/2} \left(\dfrac{\texttt{TAD}^2}{2\#\mathcal{T}_h \, |\widehat{\Delta}_K|} \right)^{1/2}, \\ \lambda_{2,K}^{opt} = g_1^{-1/2} \left(\dfrac{\texttt{TAD}^2}{2\#\mathcal{T}_h \, |\widehat{\Delta}_K|} \right)^{1/2}, \\ \mathbf{r}_{1,K}^{opt} = \mathbf{g}_2, \quad \mathbf{r}_{2,K}^{opt} = \mathbf{g}_1, \end{cases} \tag{14}$$

with $|\widehat{\Delta}_K| = |\Delta_K|/(\lambda_{1,K}\lambda_{2,K})$, $\{g_i, \mathbf{g}_i\}_{i=1,2}$ the eigen-pairs associated with the scaled matrix $G_{\Delta_K}(E_\nabla)/|\Delta_K|$, with $g_1 \geq g_2 > 0$, $\{\mathbf{g}_i\}_{i=1,2}$ orthonormal vectors. The optimal quantities, $\lambda_{i,K}^{opt}$ and $\mathbf{r}_{i,K}^{opt}$ with $i = 1, 2$, represent the input to a metric-based mesh generator since they describe the distribution of lengths and directions (i.e., the metric) of the new adapted mesh. FreeFem++ turns out to be an ideal tool for this purpose [32].

Thus, in general, we distinguish two phases, i.e., the metric computation,

$$[\lambda_1^{opt}, \lambda_2^{opt}, \mathbf{r}_1^{opt}, \mathbf{r}_2^{opt}] = \texttt{metric}(\mathcal{T}_h, \rho_h, \texttt{TAD});$$

and the mesh adaptation

$$\mathcal{T}_h^{opt} = \texttt{adaptmesh}(\mathcal{T}_h, \lambda_1^{opt}, \lambda_2^{opt}, \mathbf{r}_1^{opt}, \mathbf{r}_2^{opt}).$$

Function `metric` computes elementwise the optimal quantities in (14), so that $\lambda_i^{opt}\big|_K = \lambda_{i,K}^{opt}$ and $\mathbf{r}_i^{opt}\big|_K = \mathbf{r}_{i,K}^{opt}$, while function `adaptmesh` generates the adapted mesh matching the metric just computed [39, 26].

4.3 The whole algorithm

The MSC-SIMPATY algorithm combines, in a sequential manner, the optimization with the anisotropic mesh adaptation. This algorithm represents a variant of the one proposed in [43] and filed in the pending patent [42]. Algorithm 1 shows the pseudo code of MSC-SIMPATY. The main input parameters are: the tolerance for the optimization, TOPT, and for the mesh adaptation, TAD; the tolerance CTOL and the maximum number of iterations, kmax, to stop the whole algorithm when the mesh cardinality does

Algorithm 1 MSC-SIMPATY algorithm

Input : $\texttt{TOPT}, \texttt{TAD}, \texttt{CTOL}, \texttt{kmax}$, $C_{\max}$, $S_{\max}$ $\rho_{\min}$, $\mathcal{T}_h^0$

1: Set: $\rho_h^0 = 1$, $\texttt{k} = 0$, errM = 1+CTOL
2: **while** (errM > CTOL & k < kmax) **do**
3: $\quad \rho_h^{\texttt{k}+1} = \texttt{IPOPT}(\mathcal{M}, \nabla_\rho \mathcal{M}, \mathcal{C}, \mathcal{S}, \nabla_\rho \mathcal{C}, \nabla_\rho \mathcal{S}, \rho_h^{\texttt{k}}, \rho_{\min}, C_{\max}, S_{\max}, \texttt{Mit}^{\texttt{k}}, \texttt{TOPT}, \ldots.);$
4: $\quad [\lambda_{1,K}^{\texttt{k}+1}, \lambda_{2,K}^{\texttt{k}+1}, \mathbf{r}_{1,K}^{\texttt{k}+1}, \mathbf{r}_{2,K}^{\texttt{k}+1}] = \texttt{metric}(\mathcal{T}_h^{\texttt{k}}, \rho_h^{\texttt{k}+1}, \texttt{TAD});$
5: $\quad \mathcal{T}_h^{\texttt{k}+1} = \texttt{adaptmesh}(\mathcal{T}_h^{\texttt{k}}, \lambda_{1,K}^{\texttt{k}+1}, \lambda_{2,K}^{\texttt{k}+1}, \mathbf{r}_{1,K}^{\texttt{k}+1}, \mathbf{r}_{2,K}^{\texttt{k}+1});$
6: $\quad \text{errM} = |\#\mathcal{T}_h^{\texttt{k}+1} - \#\mathcal{T}_h^{\texttt{k}}|/\#\mathcal{T}_h^{\texttt{k}};$
7: $\quad \texttt{k} = \texttt{k} + \texttt{1};$

not change appreciably or the maximum number of iterations is reached; the upper bounds for the compliance and the stress, $C_{\max}$ and $S_{\max}$, respectively; the minimum value, $\rho_{\min}$, for the density, and the initial mesh $\mathcal{T}_h^0$. We observe that parameter $\texttt{Mit}^{\texttt{k}}$ may change throughout the iterations. In particular, in the next section, $\texttt{Mit}^{\texttt{k}}$ is set to a large value only on the first iteration so that IPOPT gets very close to the optimal solution on the initial mesh. On the contrary, a smaller value is expected to suffice for the successive iterations to strike a balance between quality of the solution and non-optimality of the mesh.

5 Verification of MSC-SIMPATY

We focus on a benchmark test case to assess Algorithm 1. We consider the topology optimization of the L-shaped bracket in Figure 1. In particular, with reference to problem (1), we have $\Omega = (0, 10]^2 \backslash [6, 10]^2$, $\Gamma_D = \{(x, y) : x \in [0, 4], y = 10\}$, $\Gamma_N = \{(x, y) : x = 10, |y-2| \leq 0.5\}$, $\Gamma_F = \partial\Omega \backslash (\Gamma_D \cup \Gamma_N)$ and $\mathbf{f} = [0, -1]^T$. The elastic parameters are set to $E = 1$ and $\nu = 0.3$, whereas we choose $p = 3$ in (4), and $\gamma = 10$ and $p_s = 0.5$ in (8).

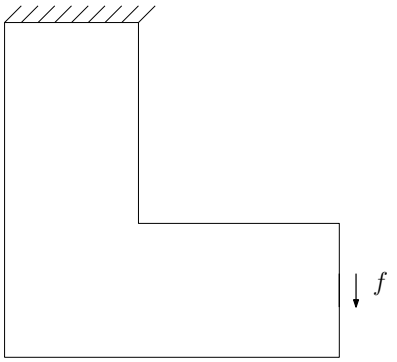

Figure 1: L-shaped bracket domain.

We consider three different scenarios:
i) only the compliance constraint in (10) is active;
ii) only the stress constraint in (10) is switched on;
iii) both the constraints in (10) are considered.
The next sections are devoted to analyze these three settings, separately. Obviously, the input parameters as well as the IPOPT syntax will be modified accordingly in the case of a mono-constrained problem.

5.1 Compliance-constrained topology optimization

We run MSC-SIMPATY algorithm, with the following input parameters: $\texttt{TOPT} = 10^{-4}$, $\texttt{TAD} = 0.15$, $\texttt{CTOL} = 0.10$, $\texttt{kmax} = 10$, $C_{\max} = 2C_0$, $C_0 = 106$ being the compliance associated with the full structure (i.e., $\rho = 1$ for any $\mathbf{x} \in \Omega$), $\rho_{\min} = 10^{-3}$ and selecting an initial uniform mesh, $\mathcal{T}_h^0$, consisting of 9546 triangles. Moreover, the parameter $\texttt{Mit}^{\texttt{k}}$ in `IPOPT` is set to 100 for $\texttt{k} = 0$ and to 15 for $\texttt{k} > 0$.

MSC-SIMPATY algorithm converges after 5 iterations, with errM= 0.077 and a final adapted mesh with 19304 elements. Figure 2 shows the corresponding density, ρ_h^5, which exhibits the expected layout, characterized by several struts hinged at the inner corner [12, 34]. This is standard for a minimum-compliance problem, where the stiffness of the configuration is increased with the introduction of substructures. The optimal layout is characterized by a remarkable mass reduction, the volume fraction being $\mathcal{M} = 0.372$, and the compliance constraint is satisfied, being $\mathcal{C} = 201.4 \leq C_{\max}$.

The benefits due to the anisotropic mesh adaptation are evident from the sharp material/void interface. Figure 3, left, shows the final adapted mesh, characterized by a maximum aspect ratio $s_K^{\max} = \max_{K \in \mathcal{T}_h} s_K = 105.83$.

Finally, in Figure 3, right, we show the results of a structural analysis, based on the von Mises yield criterion. It is evident that the maximum stress is attained around the inner corner. Notice that, in this and, analogously, in Figures 5 and 7, right panels, the values are scaled to the maximum pointwise value, $\sigma_{VM}^{\max}$, over the three scenarios, provided in Table 1. We consider as reference, the value for $\mathcal{S}$ associated with the full structure, i.e., $S_0 = 1.34$. The value for $\mathcal{S}$ on the optimized structure is 20.10. This suggests that the introduction of a stress-constraint is advisable with a view to a resistant structure.

5.2 Stress-constrained topology optimization

The input parameters to MSC-SIMPATY are now: $\texttt{TOPT} = 10^{-4}$, $\texttt{TAD} = 15$, $\texttt{CTOL} = 0.10$, $\texttt{kmax} = 10$, $S_{\max} = 5S_0$, with S_0 defined as in the previous section, $\rho_{\min} = 10^{-3}$, and $\mathcal{T}_h^0$ as in the previous scenario. Parameter $\texttt{Mit}^{\texttt{k}}$ is set to $\texttt{Mit}^0 = 320$, and $\texttt{Mit}^{\texttt{k}} = 15$ for $\texttt{k} > 0$. The initial large value for this

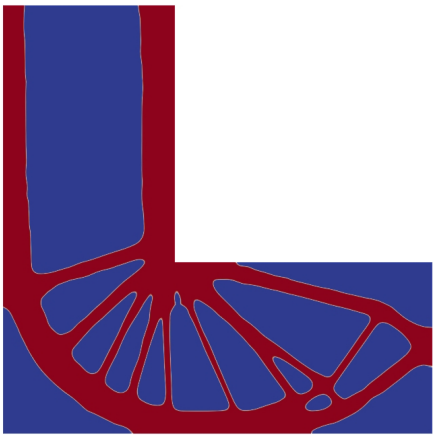

Figure 2: Compliance-constrained optimization: density distribution.

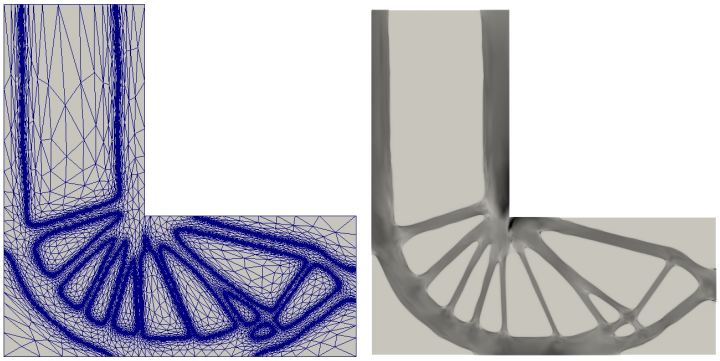

Figure 3: Compliance-constrained optimization: anisotropic adapted mesh (left) and von Mises stress distribution (right).

parameter is justified by the much slower convergence of the algorithm with respect to a compliance-constrained optimization, due to the nonlinearity associated with the stress definition.

Convergence of Algorithm 1 is achieved after 4 iterations, with the final layout characterized by a volume fraction, $\mathcal{M}$, equal to 0.369 (see Figure 4). Although this value is fully comparable with the one in the compliance-constrained case, we remark the different material distribution in the design domain. In particular, this new structure is characterized by less and thicker struts and some material removal around the inner corner.

The left panel of Figure 5 shows the anisotropic adapted mesh consisting of 17483 elements, with a maximum aspect ratio $s_K^{\max} = 120.43$, and a corresponding stagnation error errM= 0.097, while Figure 5, right, displays the von Mises stress distribution. On comparing the right panels of Figures 3 and 5, we can appreciate the reduction of the stress in correspondence with point $(4, 4)$, together with a general more homogeneous stress distribution

around this corner.

From a quantitative viewpoint, the value for $\mathcal{S}$ is 6.16, which is clearly to within the specified bound, 6.70. Concerning the compliance, we have that $\mathcal{C} = 258.64$.

A cross-comparison between a compliance-constrained and a stress-constrained settings confirms that to design a structure sufficiently resistant and stiff the two constrained have to be enforced simultaneously.

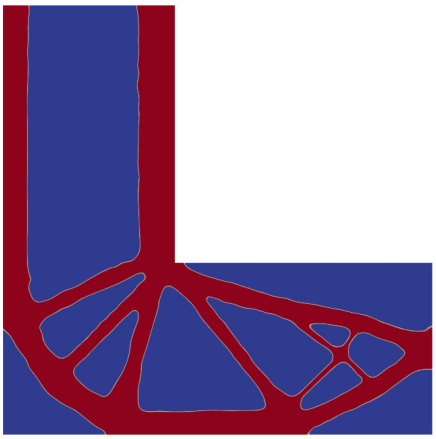

Figure 4: Stress-constrained optimization: density distribution.

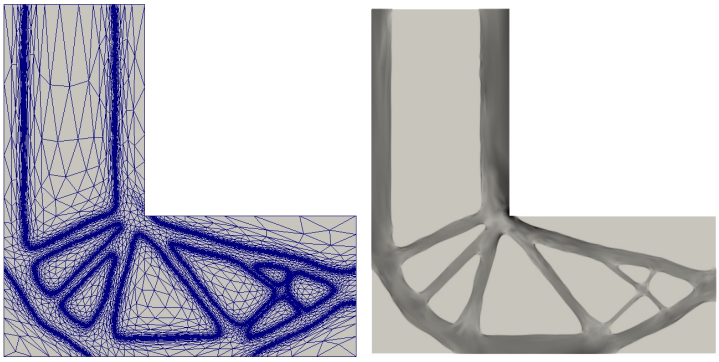

Figure 5: Stress-constrained optimization: anisotropic adapted mesh (left) and von Mises stress distribution (right).

5.3 Compliance- and stress-constrained topology optimization

We perform the last run of Algorithm 1 by selecting the following input data: `TOPT` $= 10^{-4}$, `TAD` $= 0.15$, `CTOL` $= 0.10$, `kmax` $= 10$, $C_{\max} = 2C_0$, $S_{\max} = 5S_0$, with C_0 and S_0 defined as above, $\rho_{\min} = 10^{-3}$, and the same

initial mesh, $\mathcal{T}_h^0$, as in the two previous sections. Parameter $\texttt{Mit}^{\texttt{k}}$ for IPOPT is fixed to 140 and 10 for the first and the successive iterations, respectively. The presence of the compliance constraint makes convergence faster with respect to the case in Section 5.2 so that we can decrease the value for $\texttt{Mit}^{\texttt{0}}$.

MSC-SIMPATY algorithm converges after 5 iterations with errM = 0.084. The optimized layout shown in Figure 6 is characterized by a volume fraction $\mathcal{M}$ equal to 0.371, which essentially coincides with the values obtained in the two single-constrained cases. This structure exhibits an intermediate topology compared with the ones in Figures 2 and 4. In particular, the material near the inner corner is less than the compliance-constrained case but more than the stress-constrained setting.

Both the constraints are satisfied, being $\mathcal{C} = 201.40 \leq 212$ and $\mathcal{S} = 6.69 \leq 6.70$, which confirms the reliability of the proposed procedure.

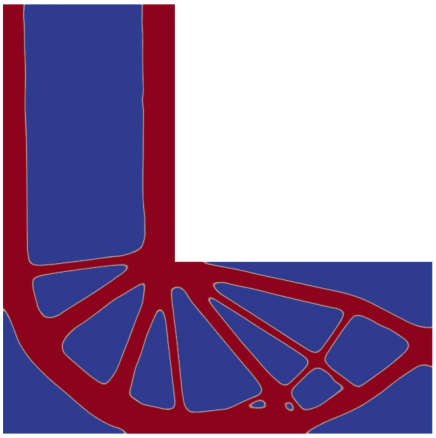

Figure 6: Compliance- and stress-constrained optimization: density distribution.

Figure 7, left, shows the final anisotropic adapted mesh, which is characterized by 12567 elements and by a maximum aspect ratio $s_K^{\max} = 102.66$. We observe that, for the same accuracy, TAD, the mesh associated with the multiple-constrained problem requires about 35% and 28% less elements than the single compliance-constrained and stress-constrained case, respectively.

Finally, the stress distribution in Figure 7, right, shows that the current structure supports a larger stress with respect to the one in Figure 4, due to the enforcement of the additional constraint on the compliance. Actually, the structure is pushed to work at its resistance limit.

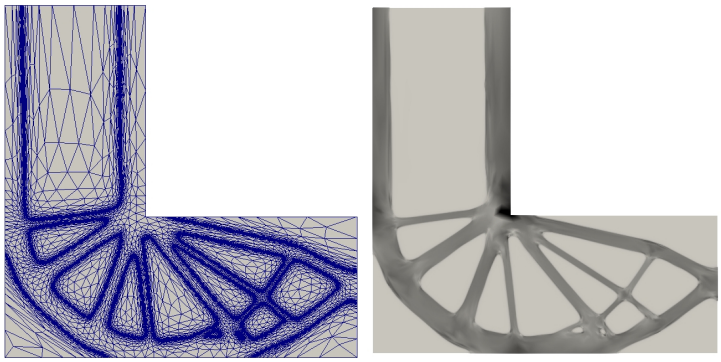

Figure 7: Compliance- and stress-constrained optimization: anisotropic adapted mesh (left) and von Mises stress distribution (right).

6 Conclusions

SIMPATY algorithm has been challenged on more realistic settings with respect to the ones in [43, 22], where the structure mass is minimized under a single- as well as a multi-constrained context. In particular, we have selected the compliance and the von Mises stress as the quantities to be controlled. This generalization led to the new MSC-SIMPATY algorithm, which preserves the advantages characterizing the original procedure. Among these, we cite the capability to sharply and smoothly capture the material/void interface and the possibility to avoid any post-processing and filtering.

As far as the structural analysis is concerned, the proposed algorithm is capable of delivering mechanically reliable structures, which make the topology more complex to meet the requirements on the compliance and properly displace the material to avoid the failure of the structure. Table 1 gathers the most meaningful quantities characterizing MSC-SIMPATY, in terms of both mechanical and algorithmic performances.

Next steps include the generalization to a 3D setting together with an extensive validation. As a preliminary attempt towards a 3D-printing process, we show in Figure 8 the 3D structures obtained by extrusion starting from the density distribution in Figure 2, 4 and 6, respectively and saved in an STL file, which is the standard format required by 3D printers. Although these are very preliminary results, we can appreciate the high smoothness of the structures and the sharp definition of their boundaries.

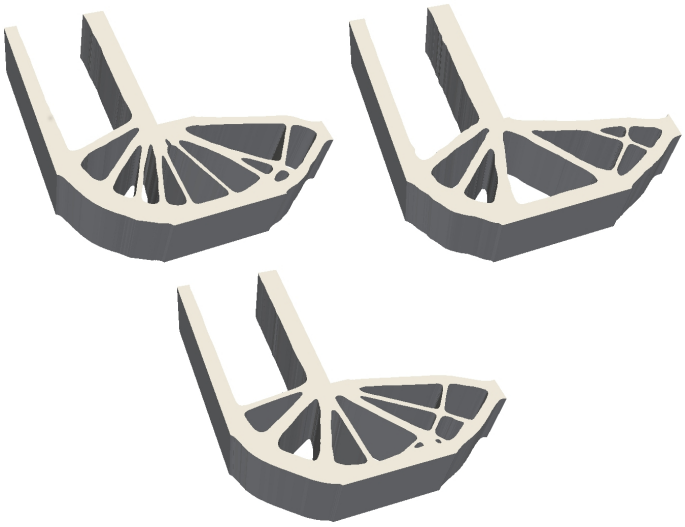

Figure 8: MSC-SIMPATY algorithm: extruded 3D structures converted in the STL file format.

	$\mathcal{C}$	$\mathcal{S}$	$\mathcal{C}+\mathcal{S}$
$\mathcal{M}$	0.372	0.369	0.371
$\mathcal{C}$	201.40	258.64	201.40
$\mathcal{S}$	20.10	6.16	6.69
$\sigma_{VM}^{\max}$	15.77	9.84	10.73
iterations	5	4	5
$\#\mathcal{T}_h$	19304	17483	12567
$s_K^{\max}$	105.83	120.43	102.66

Table 1: MSC-SIMPATY algorithm: quantitative comparison among the three optimization procedures.

References

[1] Ainsworth, M., Oden, J.T.: A Posteriori Error Estimation in Finite Element Analysis. John Wiley & Sons, New York (2000)

[2] Allaire, G., de Gournay, F., Jouve, F., Toader, A.M.: Structural optimization using topological and shape sensitivity via a level set method. Control Cybernet. **34**(1), 59–80 (2005)

[3] Allaire, G., Jouve, F., Maillot, H.: Topology optimization for minimum stress design with the homogenization method. Struct. Multidisc. Optim. **28**, 87–98 (2004)

[4] Allaire, G., Jouve, F., Toader, A.: Structural optimization using sensitivity analysis and level set-method. J. Comput. Phys. **194**, 363–393 (2004)

[5] Amstutz, S.: Connections between topological sensitivity analysis and material interpolation schemes in topology optimization. Struct. Multidiscip. Optim. **43**(6), 755–765 (2011)

[6] Bendsøe, M.P.: Optimization of Structural Topology, Shape, and Material. Springer-Verlag, Berlin (1995)

[7] Bendsøe, M.P., Kikuchi, N.: Generating optimal topologies in structural design using a homogenization method. Comput. Methods Appl. Mech. Engrg. **71**(2), 197–224 (1988)

[8] Bendsøe, M.P., Sigmund, O.: Topology Optimization: Theory, Methods and Applications. Springer-Verlag, Berlin Heidelberg (2003)

[9] Bourdin, B.: Filters in topology optimization. Internat. J. Numer. Methods Engrg. **50**(9), 2143–2158 (2001)

[10] Bourdin, B., Chambolle, A.: Design-dependent loads in topology optimization. ESAIM Control. Optim. Calc. Var. **9**, 19–48 (2003)

[11] Bruggi, M., Cinquini, C.: Topology optimization for thermal insulation: an application to building engineering. Eng. Optim. **43**(11), 1223–1242 (2011)

[12] Bruggi, M., Duysinx, P.: Topology optimization for minimum weight with compliance and stress constraints. Struct. Multidiscip. Optim. **46**(3), 369–384 (2012)

[13] Burger, M., Hackl, B., Ring, W.: Incorporating topological derivatives into level set methods. J. Comput. Phys. **194**(1), 344–362 (2004)

[14] Burger, M., Osher, S.J.: A survey on level set methods for inverse problems and optimal design. European J. Appl. Math. **16**(2), 263–301 (2005)

[15] Burger, M., Stainko, R.: Phase-field relaxation of topology optimization with local stress constraints. SIAM J. Control Optim. **45**(4), 1447–1466 (2006)

[16] Cai, S., Zhang, W.: Stress constrained topology optimization with free-form design domains. Comput. Methods Appl. Mech. Engrg. **289**, 267–290 (2015)

[17] Dedè, L., Borden, M.J., Hughes, T.J.R.: Isogeometric analysis for topology optimization with a phase field model. Arch. Comput. Methods Eng. **19**(3), 427–465 (2012)

[18] Dompierre, J., Vallet, M.G., Bourgault, Y., Fortin, M., Habashi, W.G.: Anisotropic mesh adaptation: towards user-independent, mesh-independent and solver-independent CFD. III. Unstructured meshes. Internat. J. Numer. Methods Fluids **39**(8), 675–702 (2002)

[19] Ern, A., Guermond, J.L.: Theory and Practice of Finite Elements, vol. 159. Springer-Verlag, New York (2004)

[20] Eschenauer, H.A., Olhoff, N.: Topology optimization of continuum structures: A review. Appl. Mech. Rev. **54**(4), 331–390 (2001)

[21] Farrell, P.E., Micheletti, S., Perotto, S.: An anisotropic Zienkiewicz-Zhu-type error estimator for 3D applications. Int. J. Numer. Meth. Engng **85**(6), 671–692 (2011)

[22] Ferro, N., Micheletti, S., Perotto, S.: POD-assisted strategies for structural topology optimization. Comput. Math. Appl. **77**(10), 2804–2820 (2019)

[23] Ferro, N., Micheletti, S., Perotto, S.: Density-based inverse homogenization with anisotropically adapted elements. In: A. Corsini, S. Perotto, G. Rozza, H. van Brummelen (eds.) *Lect. Notes Comput. Sci. Eng. Series*, Proceedings of the 19th International Conference on Finite Elements in Flow Problems. Springer (2020)

[24] Formaggia, L., Micheletti, S., Perotto, S.: Anisotropic mesh adaption with application to CFD problems. In: H. Mang, F. Rammerstorfer, J. Eberhardsteiner (eds.) Proceedings of WCCM V, Fifth World Congress on Computational Mechanics, pp. 1481–1493 (2002)

[25] Formaggia, L., Perotto, S.: New anisotropic a priori error estimates. Numer. Math. **89**(4), 641–667 (2001)

[26] Frey, P.J., George, P.L.: Mesh Generation. Application to Finite Elements, second edn. ISTE, London; John Wiley & Sons, Inc., Hoboken, NJ (2008)

[27] G. Alaimo F. Auricchio, M.C., Zingales, M.: Multi-objective optimization of nitinol stent design. Medical Engineering and Physics **47**, 13–24 (2017)

[28] Giacomini, M., Pantz, O., Trabelsi, K.: Volumetric expressions of the shape gradient of the compliance in structural shape optimization (2017). ArXiv:1701.05762

[29] Gomes, A.A., Suleman, A.: Application of spectral level set methodology in topology optimization. Struct. Multidiscip. Optim. **31**(6), 430–443 (2006)

[30] Gould, P.L.: Introduction to Linear Elasticity. Springer–Verlag, New York (1994)

[31] Habashi, W.G., Dompierre, J., Bourgault, Y., Ait-Ali-Yahia, D., Fortin, M., Vallet, M.G.: Anisotropic mesh adaptation: towards user-independent, mesh-independent and solver-independent CFD. I. General principles. Internat. J. Numer. Methods Fluids **32**(6), 725–744 (2000)

[32] Hecht, F.: New development in FreeFem++. J. Numer. Math. **20**(3-4), 251–265 (2012)

[33] Huang, X., Xie, Y.M., Jia, B., Li, Q., Zhou, S.W.: Evolutionary topology optimization of periodic composites for extremal magnetic permeability and electrical permittivity. Struct. Multidiscip. Optim. **46**(3), 385–398 (2012)

[34] Jensen, K.E.: Solving stress and compliance constrained volume minimization using anisotropic mesh adaptation, the method of moving asymptotes and a global p-norm. Struct. Multidiscip. Optim. **54**(4), 831–841 (2016)

[35] Lazarov, B.S., Sigmund, O.: Filters in topology optimization based on Helmholtz-type differential equations. Int. J. Numer. Meth. Engng **86**(6), 765–781 (2011)

[36] Liang, Q.: Performance-based Optimization of Structures. Theory and Applications. Spon Press, London (2005)

[37] M. Collet, M.B., Duysinx, P.: Topology optimization for minimum weight with compliance and simplified nominal stress constraints for fatigue resistance. Struct. Multidisc. Optim. **55**(3), 839–855 (2017)

[38] M. Wang, X.W., Guo, D.: A level set method for structural topology optimization. Comput. Methods Appl. Mech. Eng. **192**(1-2), 227–246 (2003)

[39] Micheletti, S., Perotto, S.: Reliability and efficiency of an anisotropic Zienkiewicz-Zhu error estimator. Comput. Methods Appl. Mech. Engrg. **195**(9–12), 799–835 (2006)

[40] Micheletti, S., Perotto, S.: Anisotropic adaptation via a Zienkiewicz-Zhu error estimator for 2D elliptic problems. In: G. Kreiss, P. Lötstedt, A. Målqvist, M. Neytcheva (eds.) Numerical Mathematics and Advanced Applications, pp. 645–653. Springer-Verlag Berlin Heidelberg (2010)

[41] Micheletti, S., Perotto, S., Farrell, P.E.: A recovery-based error estimator for anisotropic mesh adaptation in CFD. Bol. Soc. Esp. Mat. Apl. SeMA **50**, 115–137 (2010)

[42] Micheletti, S., Perotto, S., Soli, L.: Ottimizzazione topologica adattativa per la fabbricazione stratificata additiva (2017). Italian patent application No. 102016000118131, filed on November 22, 2016 (extended as *Adaptive topology optimization for additive layer manufacturing*, International patent application PCT No. PCT/IB2017/057323)

[43] Micheletti, S., Perotto, S., Soli, L.: Topology optimization driven by anisotropic mesh adaptation: Towards a free-form design. Computers & Structures **214**, 60 – 72 (2019)

[44] Munk, D.J., Vio, G.A., Steven, G.P.: Topology and shape optimization methods using evolutionary algorithms: a review. Struct. Multidiscip. Optim. **52**(3), 613–631 (2015)

[45] Rozvany, G.I.N.: A critical review of established methods of structural topology optimization. Struct. Multidiscip. Optim. **37**, 217–237 (2009)

[46] Schwerdtfeger, J., Wein, F., Leugering, G., Singer, R.F., Körner, C., Stingl, M., Schury, F.: Design of auxetic structures via mathematical optimization. Adv. Mater. **23**(22-23), 2650–2654 (2011)

[47] Sigmund, O., Petersson, J.: Numerical instabilities in topology optimization: a survey on procedures dealing with checkerboards, mesh-dependencies and local minima. Struct. Optim. **16**(1), 68–75 (1998)

[48] Sokolowski, J., Zochowski, A.: On the topological derivative in shape optimization. SIAM J. Control. Opt. **37**, 1251–1272 (1999)

[49] Svanberg, K.: The method of moving asymptotes-a new method for structural optimization. Int. J. Numer. Meth. Engng **24**(2), 359–373 (1987)

[50] Villanueva, C.H., Maute, K.: CutFEM topology optimization of 3D laminar incompressible flow problems. Comput. Methods Appl. Mech. Engrg. **320**, 444–473 (2017)

[51] Wächter, A., Biegler, L.T.: On the implementation of an interior-point filter line-search algorithm for large-scale nonlinear programming. Math. Program. **106**(1, Ser. A), 25–57 (2006)

[52] Xie, Y., Steven, G.: A simple evolutionary procedure for structural optimization. Comput. Struct. **49**, 885–896 (1993)

[53] Yoon, G.H.: Structural topology optimization for frequency response problem using model reduction schemes. Comput. Methods Appl. Mech. Engrg. **199**(25-28), 1744–1763 (2010)

[54] Zargham, S., Ward, T., Ramli, R., Badruddin, I.: Topology optimization: a review for structural designs under vibration problems. Struct. Multidisc. Optim. **53**(6), 1157–1177 (2016)

[55] Zienkiewicz, O.C., Zhu, J.Z.: A simple error estimator and adaptive procedure for practical engineering analysis. Int. J. Numer. Meth. Engng **24**, 337–357 (1987)

[56] Zienkiewicz, O.C., Zhu, J.Z.: The superconvergent patch recovery and a posteriori error estimates. II: Error estimates and adaptivity. Int. J. Numer. Meth. Engng **33**, 1365–1382 (1992)

MOX Technical Reports, last issues

Dipartimento di Matematica
Politecnico di Milano, Via Bonardi 9 - 20133 Milano (Italy)

02/2020 Fresca, S.; Dede', L.; Manzoni, A.
A comprehensive deep learning-based approach to reduced order modeling of nonlinear time-dependent parametrized PDEs

01/2020 Pozzi, S.; Vergara, C.
Mathematical and numerical models of atherosclerotic plaque progression in carotid arteries

60/2019 Ieva, F; Paganoni, A.M.; Romo, J.; Tarabelloni, N.
roahd Package: Robust Analysis of High Dimensional Data

59/2019 Antonietti, P.F; Manzini, G.; Mourad, H.M.; Verani, M.
The virtual element method for linear elastodynamics models. Design, analysis, and implementation

58/2019 Antonietti, P.F; Manzini, G.; Mourad, H.M.; Verani, M.
The virtual element method for linear elastodynamics models. Design, analysis, and implementation

57/2019 Antonietti, P.F.; Bertoluzza, S.; Prada, D.; Verani M.
The Virtual Element Method for a Minimal Surface Problem

56/2019 Antonietti, P.F.; Berrone, S.; Borio A.; D'Auria A.; Verani, M.; Weisser, S.
Anisotropic a posteriori error estimate for the Virtual Element Method

54/2019 Simona, A.; Bonaventura, L; de Falco, C.; Schoeps, S.
IsoGeometric Approximations for Electromagnetic Problems in Axisymmetric Domains

55/2019 Agosti, A.; Ciarletta, P.; Garcke, H.; Hinze, M.
Learning patient-specific parameters for a diffuse interface glioblastoma model from neuroimaging data

52/2019 Cerroni, D.; Radu, A. R. ; Zunino, P.
Numerical solvers for a poromechanic problem with a moving boundary